

Further evidence to support a tidal disruption event in the changing-look AGN SDSS J0159

Xue-Guang Zhang^{*}

School of physics and technology, Nanjing Normal University, No. 1, Wenyuan Road, 210046, P. R. China

ABSTRACT

In this Letter, we report further evidence to support a tidal disruption event (TDE) in the known changing-look AGN SDSS J0159, through the unique variabilities of asymmetric broad H α : broader but redder in 2010 than in 2000. Accepted the broad H α emission regions tightly related to accreting debris in a central TDE, the well-known relativistic accretion disk origination can be applied to well explain the asymmetric broad H α variabilities in SDSS J0159. Moreover, the model determined broad H α emission regions have the sizes not follow the empirical R-L relation valid in normal broad line AGN, but have locations basically similar to the regions of accreting debris from a central TDE in SDSS J0159, indicating tight connections between the broad H α emission materials and central TDE debris. Therefore, explanations of the asymmetric broad H α variabilities through the relativistic accretion disk origination provide further clues to support a central TDE in SDSS J0159.

Key words: galaxies:active - galaxies:nuclei - quasars:emission lines - transients:tidal disruption events

1 INTRODUCTION

TDEs (Tidal Disruption Events) have been studied in detail for more than four decades (Rees 1988; Loeb & Ulmer 1997; Gezari et al. 2012; Guillochon & Ramirez-Ruiz 2013; Guillochon et al. 2014; Holoien et al. 2016; Wang et al. 2018; Thorp et al. 2019), with accreting fallback debris from stars tidally disrupted by central black holes (BHs) leading to expected time-dependent apparent variabilities. And based on long-term variability properties, and there are more than 80 TDEs detected and reported (see detailed information in <https://tde.space/>), strongly supporting TDEs as better indicators to massive BHs and corresponding BH accreting systems. More recent reviews on TDEs can be found in Stone et al. (2018). Based on well improved theoretical TDEs in Guillochon & Ramirez-Ruiz (2013); Guillochon et al. (2014), accreting fallback debris in TDEs have apparent time-dependent structure evolutions, also leading to structure evolutions of broad emission line regions (BLRs) built from accreting TDE debris.

Besides direct results on both observational and theoretical TDEs, there is one special kind of broad line AGN (Active Galactic Nuclei), AGN with double-peaked broad low-ionization emission lines (double-peaked AGN) (Chen et al. 1989; Eracleous et al. 1995; Strateva et al. 2003; Flohic & Eracleous 2008; Zhang & Feng 2017), with accreting debris in TDEs as one probable origination of emission materials of double-peaked broad emission lines (see discussions in Eracleous et al. (1995), also see simulated results on BLRs from TDE debris in Guillochon et al. (2014)). Therefore, if observed broad emission lines were related to TDEs, broad emission lines could be explained by reasonable disk-like BLRs related to TDEs, which is the main objective of the Letter.

More recently, among the reported TDEs candidates, Liu et al. (2017) have reported a relativistic elliptical accretion model well

applied to describe three-month variabilities of the observed double-peaked broad H α in PTF09dj. Holoien et al. (2019) have shown a non-axisymmetric accretion disk model applied to describe two-month variabilities of the observed double-peaked broad H α in PS18kh. Short et al. (2020) have shown that the seven-month variabilities of broad Balmer lines have an asymmetric double-peaked phase which is consistent with accretion disc emissions in AT 2018hyz. Hung et al. (2020) have also shown that the distinct double-peaked broad H α can be well described by a low eccentricity accretion disk emissions in the AT 2018hyz. Meanwhile, Holoien et al. (2016) have shown four-month variabilities of asymmetric broad H α (apparently asymmetric features shown in Fig. 8 in Holoien et al. (2016)) in ASASSN-14li. Therefore, accreting debris in TDEs can lead to double-peaked broad emission features related to disk-like emission regions. And apparently, the double-peaked features reported above are transient features that survive for less than 1 year, basically consistent with durations of TDEs determined by central BH masses around $10^6 M_{\odot}$ and parameters of disrupted solar-like main-sequence stars. Different parameters in TDEs, such as different ratios of the tidal radius to the pericenter distance, different central BH mass and stellar properties, etc., could lead to expected double-peaked features persisted for longer durations, such as the case in the TDE candidate SDSS J0159 with ten-year variability of asymmetric broad H α .

Merloni et al. (2015) have shown the observed broad H α in SDSS J0159 (=J015957.64+003310.5) in 2000 and 2010, and reported interesting variabilities in ten years: broad H α in 2010 with FWHM (Full Width at Half Maximum) about 6167km/s wider than that in 2000 with FWHM about 3408km/s and central wavelength in 2000 with λ_0 about 6560Å bluer than that in 2010 with λ_0 about 6582Å. The special variability properties of broad H α in SDSS J0159, especially the different central wavelengths, can not be clearly explained by common variabilities of broad emission lines coming from normal BLRs in normal AGN, however, accretion disk origination of

^{*} Corresponding author Email: xgzhang@njnu.edu.cn

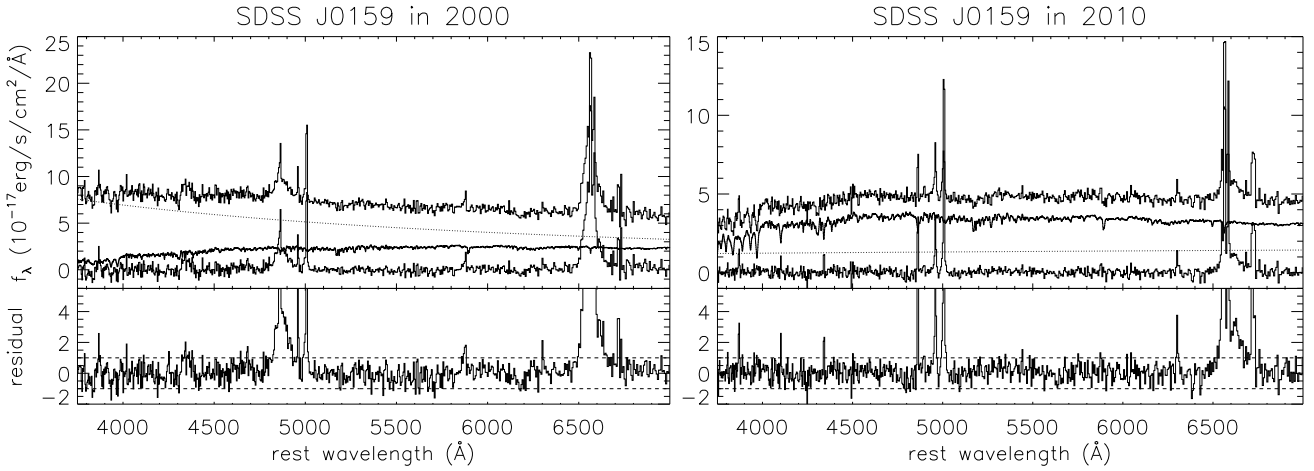


Figure 1. On the determined stellar lights by the SSP method (top panels) and the corresponding residuals (bottom panels) in the SDSS spectrum in 2000 (left panels) and in 2010 (right panels). In each top panel, from top to bottom, thin solid line, thick dotted line, thick solid line and thin solid line represent the observed spectrum, the determined power law AGN continuum emissions, the determined stellar lights and the pure line spectrum, respectively. In each bottom panel, thick horizontal dashed lines show $residual = \pm 1$.

broad $H\alpha$ related to TDEs could provide reasonable explanations to the observed broad $H\alpha$ variabilities in SDSS J0159. Meanwhile, we have recently reported properties of BH mass in SDSS J0159 in Zhang et al. (2019) that there are different virial BH mass under the virialization assumption (Peterson et al. 2004) from the BH mass estimated through the $M_{BH} - \sigma$ relation (Kormendy & Ho 2015). The different BH masses through different methods strongly indicate that there should be strong contributions to broad line emission materials from central TDE debris. Therefore, the known changing-look AGN SDSS J0159 is a better target to discuss probable connections between its ten-year long variabilities of asymmetric broad $H\alpha$ and a central TDE. Section 2 presents our main results on variabilities of broad $H\alpha$ of SDSS J0159, and necessary discussions. Section 3 gives our final conclusions.

2 BROAD $H\alpha$ VARIABILITY IN SDSS J0159

Spectra of SDSS J0159 in 2000 and 2010 have been collected by PLATE-MJD-FIBERID of 0403-51871-0549 and 3609-55201-0524 from SDSS. Then, the following steps have been applied to subtract contributions of both stellar lights and narrow emission lines in the SDSS spectra, in order to obtain the pure broad $H\alpha$. Here, the widely accepted SSP method (Simple Stellar Population) (Bruzual & Charlot 2003; Kauffmann et al. 2003) has been applied to determine contributions of stellar lights in the observed spectrum with emission lines being masked out, considering broadened stellar templates plus one power-law component for the AGN continuum emissions. Meanwhile, we are very familiar with the SSP method, such as what we have recently done in Zhang et al. (2019), and do not show further discussions on the SSP method any more. Fig. 1 shows the SSP method determined stellar lights through the Levenberg-Marquardt least-squares minimization technique, and the corresponding residuals of $\frac{y - y_m}{y_{err}}$ where y , y_m and y_{err} represent the observed spectrum after emission lines being masked out, the determined best fitted results and the corresponding errors of y , respectively. Similar results on subtractions of the stellar lights can be found for SDSS J0159 in LaMassa et al. (2015).

After subtractions of the stellar lights, multi-Gaussian components

have been applied to describe the emission lines around $H\alpha$ within rest wavelength from 6400Å to 6850Å. There are two broad Gaussian components applied to describe the broad $H\alpha$, and five another narrow Gaussian components applied to describe the other narrow emission lines of narrow $H\alpha$, [N II] and [S II] doublets. Similar emission line fitting procedure has been applied in our more recent paper Zhang & Feng (2017b). Fig. 2 shows the best fitted results and corresponding residuals to the emission lines around $H\alpha$ through the Levenberg-Marquardt least-squares minimization technique. The determined $\chi^2 = SSR/DoF$ values (SSR and DoF as summed squared residuals and degree of freedom) are about ~ 1.31 and ~ 1.08 for the best fitted results to the emission lines in 2000 and in 2010, respectively. Table 1 lists the determined line parameters of broad and narrow emission lines. Here, λ_0 (first moment) and σ (second moment) of the broad $H\alpha$ are determined by

$$\lambda_0 = \frac{\int \lambda \times f_\lambda d\lambda}{\int f_\lambda d\lambda} \quad \sigma^2 = \frac{\int \lambda^2 \times f_\lambda d\lambda}{\int f_\lambda d\lambda} - \lambda_0^2 \quad (1)$$

, where f_λ represents line profile of the broad $H\alpha$. The uncertainties of λ_0 and σ and line flux are determined by the bootstrap method.

The redder and broader broad $H\alpha$ in 2010 can be re-confirmed, as reported in Merloni et al. (2015). Meanwhile, Table 1 also lists the information of the two broad Gaussian components shown as blue dashed lines in Fig. 2. There are one blue component plus one red component in 2000, but two red components with much different line widths in 2010, strongly indicating that it is unreasonable to consider rotating independent double emission regions to explain the two Gaussian components. Therefore, the main objective of two Gaussian components to the broad $H\alpha$ is only to determine the best fitted results to the emission lines around $H\alpha$ (especially to the narrow emission lines), and the asymmetric line profiles of broad $H\alpha$ shown in Fig. 3 can be well determined after subtractions of both the narrow emission lines and the power-law continuum emissions from the line spectra shown in Fig. 2. Then, the following accretion disk model is mainly considered.

Different kinds of relativistic accretion disk models can be found in the literature. Circular accretion disk model has been firstly proposed in Chen et al. (1989), and then the improved elliptical accretion disk model can be found in Eracleous et al. (1995). Besides the circular

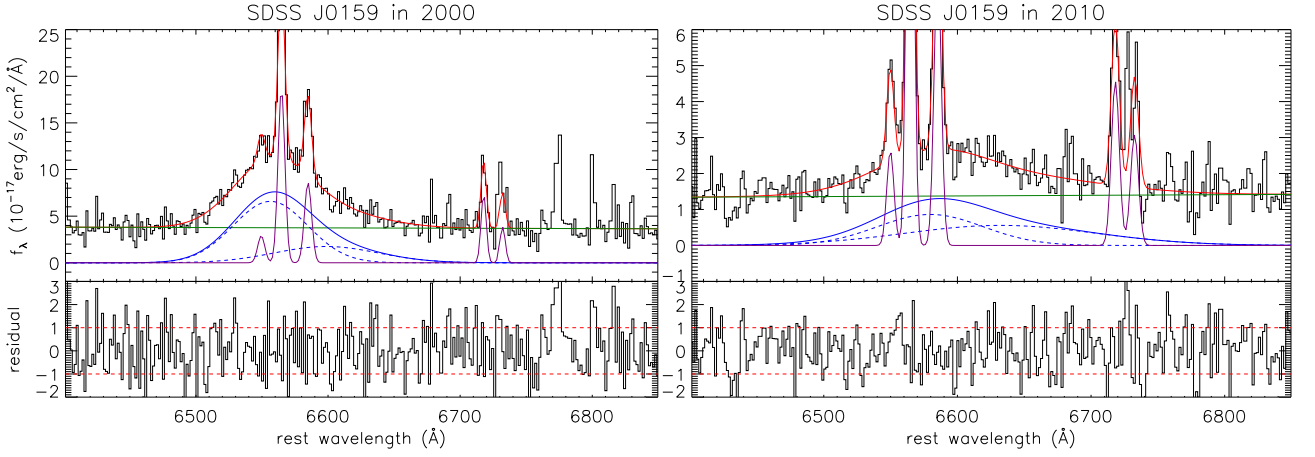


Figure 2. The best fitted results (top panels) and the corresponding residuals (bottom panels) to the emission lines around H α in 2000 (left panels) and in 2010 (right panels) by multiple Gaussian functions, after subtractions of the stellar lights. In each top panel, black solid line and red solid line show the line spectrum and the best fitted results, dark green solid line shows the determined power law AGN continuum emissions, blue solid line shows the determined broad H α , purple solid lines show the determined narrow H α , [N II] and [S II] doublets, and blue dashed lines show the two Broad Gaussian components included in the broad H α . In each bottom panel, red dashed lines show $residual = \pm 1$.

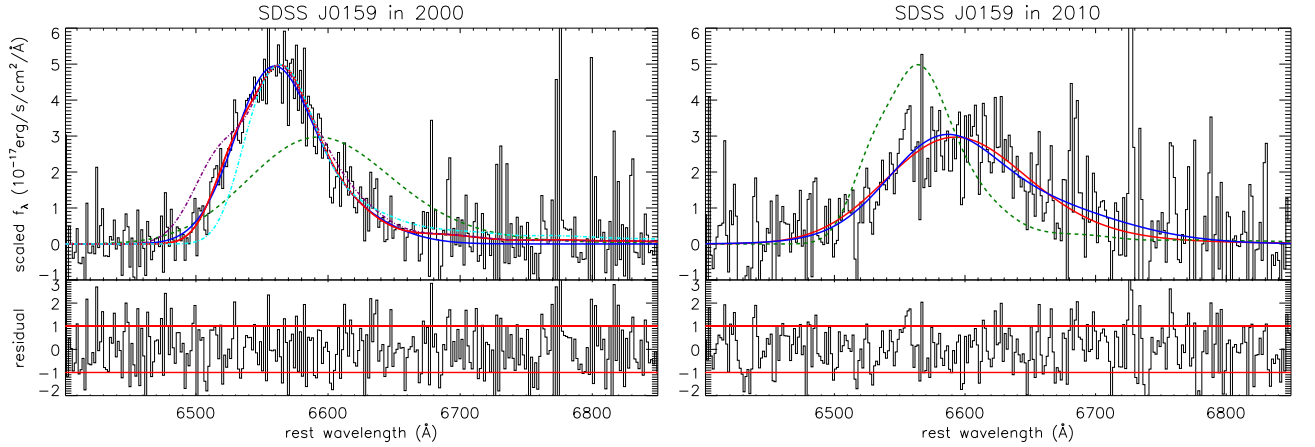


Figure 3. The best fitted results (top panels) and the corresponding residuals (bottom panels) to the broad H α in 2000 (left panels) and in 2010 (right panels) by the relativistic elliptical accretion disk model, after subtractions of both the narrow emission lines and the power law AGN continuum emissions from the line spectra shown in Fig. 2. In each top panel, black solid line and red solid line represent the pure broad H α and the best fitted results by the accretion disk model, dark green dashed line shows the determined best fitted results to the broad H α observed in the other epoch by the accretion disk model, blue solid line shows the scaled Gaussian fitted results to the broad H α shown in Fig. 2. In the left panel, dot-dashed line in purple (in cyan) shows the model created line profile with $\sin(i) = 0.196 + 3 \times 0.011$ ($e_1 = 0.93 - 3 \times 0.03$), but with the other parameters set to the model determined values. In each bottom panel, horizontal red solid lines show $residual = \pm 1$.

and elliptical accretion disk models, a model of circular disk with spiral arms can be found in Storchi-Bergmann et al. (2003), a warped accretion disk model can be found in Hartnoll & Blackman (2000), and a stochastically perturbed accretion disk model can be found in Flohic & Eracleous (2008). Here, the elliptical accretion disk model is preferred, because the model with less number of necessary model parameters can explain almost all observational double-peaked features. Moreover, as the shown smooth profiles of asymmetric broad H α in SDSS J0159, it is not necessary to consider existences of arms and/or warped structures and/or bright spots which are mainly applied to subtle structures of broad line profiles (such as some cusps around peaks/shoulders). Detailed descriptions of the relativistic elliptical accretion disk model with seven model parameters can be

found in Eracleous et al. (1995). Meanwhile, we have also applied the very familiar elliptical accretion disk model, see our studies on double-peaked lines in Wang et al. (2005); Zhang (2013, 2015).

There are seven necessary model parameters (*par*): inner boundary r_0 , out boundary r_1 , inclination angle i of disk-like BLRs, eccentricity e and orientation angle ϕ_0 of elliptical rings, local broadening velocity σ_L , line emissivity slope q ($f_r \propto r^{-q}$). Then, the relativistic elliptical accretion disk model with r_0 well extended down to $\sim 6R_G$ can be applied to **simultaneously** describe the asymmetric broad H α in 2000 and in 2010 as follows. The line profiles of broad H α in 2000 and in 2010 are $[\lambda_1, f_{\lambda, 1}]$, $[\lambda_2, f_{\lambda, 2}]$, respectively, leading to a combined line profile as $[\lambda, f_{\lambda}]$ with $\lambda = [\lambda_1, \lambda_2]$ and $f_{\lambda} = [f_{\lambda, 1}, f_{\lambda, 2}]$. Then, the model expected line profile can be written as $[\lambda_M, f_{\lambda, M}]$

Table 1. Line parameters of emission lines

| Emission lines in 2000 | | | |
|------------------------|---------------------|-------------------|-------------------------------------|
| Line | λ_0 Å | σ Å | flux $10^{-17}\text{erg/s/cm}^2$ |
| Broad H α | 6568.91±6.45 | 38.12±3.26 | 654±64 |
| 1st Broad | 6556.41±10.01 | 28.21±8.19 | 460* |
| 2nd Broad | 6598.64±10.63 | 39.24±11.31 | 170* |
| Narrow H α | 6564.74±0.12 | 2.57±0.13 | 120±6 |
| [N II] λ 6583Å | 6584.85±0.24 | 2.71±0.28 | 58±7 |
| [S II] λ 6716Å | 6717.82±0.22 | 2.01±0.22 | 37±4 |
| [S II] λ 6732Å | 6732.21±0.23 | 2.01±0.22 | 19±5 |
| Emission lines in 2010 | | | |
| Broad H α | 6595.88±3.52 | 56.29±4.52 | 168±15 |
| 1st Broad | 6579.73±8.63 | 39.54±14.19 | 85* |
| 2nd Broad | 6632.25±8.74 | 71.04±25.73 | 100* |
| Narrow H α | 6564.71±0.06 | 2.53±0.05 | 117±3 |
| [N II] λ 6583Å | 6585.23±0.12 | 2.79±0.12 | 56±3 |
| [S II] λ 6716Å | 6718.17±0.17 | 3.10±0.16 | 36±2 |
| [S II] λ 6732Å | 6732.55±0.17 | 3.11±0.16 | 25±3 |

Notice: The second, third and fourth column show the central wavelength in unit of Å in rest frame, the line width (second moment) in unit of Å and the line flux in unit of $10^{-17}\text{erg/s/cm}^2$. "1st Broad" and "2nd Broad" shows the parameters of the two broad Gaussian components included in the broad H α . The symbol * means the determined uncertainties larger than the measured parameter by the least-squares minimization technique, due to lower spectral quality.

with $\lambda_M = [\lambda_1, \lambda_2]$ and $f_{\lambda, M} = [M_{par1}, M_{par2}]$. Each model determined line profile of M_{par1} and M_{par2} has seven model parameters, however, due to the accepted almost same regions and same inclination angle of the disk-like BLRs for the broad H α in 2000 and in 2010, there are finally 11 model parameters as follows: r_0 , r_1 and i for the inner and outer boundaries and the inclination angle of the disk-like BLRs, q_1 and q_2 as the line emissivity slopes for the broad H α in 2000 and in 2010, $\sigma_{L,1}$ and $\sigma_{L,2}$ as the local broadening velocities for the broad H α in 2000 and in 2010, e_1 , e_2 and $\phi_{0,1}$ and $\phi_{0,2}$ as the eccentricities and orientation angles for the disk-like BLRs of the broad H α in 2000 and in 2010. Meanwhile, due to weaker broad H α in 2010 as shown in Fig. 2, mean line intensities of pure broad H α in 2000 and 2010 are applied to scale the broad H α in 2000 and 2010, leading to the scaled broad H α in 2000 and 2010 having similar line intensities. Then, through the Levenberg-Marquardt least-squares minimization technique, the best fitted results with $\chi^2 \sim 1.21$ and the corresponding residuals to the broad H α can be well determined and shown in Fig. 3, strongly indicating the relativistic elliptical accretion disk model is an appropriate model.

The model parameters are determined as $r_0 \sim 10.5 \pm 1.1R_G$, $r_1 \sim 129.6 \pm 31.7R_G$ ¹, $\sin(i) \sim 0.196 \pm 0.011$ (about 11.3°), $q_1 \sim 1.82 \pm 0.19$, $q_2 \sim 0.72 \pm 2.13$ ², $\sigma_{L,1} \sim 730 \pm 96\text{km/s}$, $\sigma_{L,2} \sim 2230 \pm 762\text{km/s}$, $e_1 \sim 0.93 \pm 0.03$, $e_2 \sim 0.88 \pm 0.46$, $\phi_{0,1} \sim -31 \pm 2^\circ$ and $\phi_{0,2} \sim 44 \pm 60^\circ$. In addition, the model determined disk-like BLRs with a small inclination angle (nearly face on)

¹ Even different r_1 in model functions applied to emission regions of broad H α in 2000 and in 2010, similar r_1 can be found, but with larger uncertainties.

² Probably due to lower spectral quality of broad H α in 2010, the determined model parameters of q_2 and $\phi_{0,2}$ have their model determined values smaller than their corresponding uncertainties.

reasonably lead to the observed single-peaked asymmetric broad H α in SDSS J0159. Moreover, among the determined model parameters, $\sin(i)$ and e_1 have quite smaller uncertainties, mainly due to more sensitively dependence on $\sin(i)$ and e_1 . In order to show further information on the tightly constrained parameters of $\sin(i)$ and e_1 , two additional model created profiles have been shown in the left panel of Fig. 3: one is created through the elliptical accretion disk model applied with the value of $\sin(i)$ to be $\sin(i) = 0.196 + 3 \times 0.011$ (where 0.011 is the determined uncertainty of $\sin(i)$) and with the other parameters set to the model determined values, the other one is created with the value of e_1 to be $e_1 = 0.93 - 3 \times 0.03$ (where 0.03 is the determined uncertainty of e_1) and with the other parameters to the model determined values. It is clear that smaller deviations from the model determined values of $\sin(i)$ and e_1 could lead to the worse model determined profiles to describe the asymmetric broad H α . Therefore, the smaller uncertainties of $\sin(i)$ and e_1 can be well accepted. Meanwhile, we can find that the model determined parameters are different from the statistical results on disk-like BLRs in a large sample of double-peaked SDSS AGN in [Strateva et al. \(2003\)](#), especially the smaller inner and outer boundaries and larger eccentricity which will instead provide further clues on special properties of the disk-like BLRs in SDSS J0159.

Before proceeding further, there is one interesting point we should note. In the Letter, the applied relativistic elliptical accretion disk model is the one well discussed in [Eracleous et al. \(1995\)](#), a bit different from the model discussed in [Liu et al. \(2017\)](#), such as the parameter of line emissivity slope as a free model parameter in our applied model but fixed in the model discussed in [Liu et al. \(2017\)](#). Actually, if the parameter of q is fixed to 3 in the applied accretion disk model, the re-determined best fitted results could lead to $\chi^2 \sim 1.58$ larger than $\chi^2 \sim 1.21$ for the model with q as a free model parameter, indicating dependence of the results on q . Therefore, q as a free model parameter can be preferred and lead to more appropriate final best fitted results. And, it is very interesting to find that the model determined eccentricity is large and inner boundary is small for the disk-like BLRs in SDSS J0159, but similar as the reported results in [Liu et al. \(2017\)](#) with $e \sim 0.96$ and $r_0 \sim 11R_G$ for the disk-like broad line emission regions in PTF09dj. However, there are larger inner boundaries and smaller eccentricities of the determined disk-like regions with $r_0 \sim 1000R_G$ and $e \sim 0.1$ in AT 2018hyz and with $r_0 \sim 60R_G$ and $e \sim 0.25$ in PS18kh. Comparing the disk parameters in the TDEs candidates indicate the preferred elliptical accretion disk-like BLRs related to a central TDE in SDSS J0159 similar as the case in PTF09dj, but quite different from the cases in AT 2018hyz and PS18kh, mainly due to different geometric structures from TDEs with different physical parameters.

Moreover, before giving the necessary discussions, we give some detailed arguments on the important parameter of BH mass in SDSS J0159. As discussed in [Merloni et al. \(2015\)](#); [LaMassa et al. \(2015\)](#), the virial BH mass about $10^8 M_\odot$ has been reported. However, [Zhang et al. \(2019\)](#) and [Wevers et al. \(2019\)](#) have shown that the stellar velocity dispersion in SDSS J0159 is smaller than the expected value from the virial BH mass through the $M_{BH} - \sigma$ relation. If the smaller stellar velocity dispersions were accepted that $\sigma \sim 80\text{km/s}$ in [Zhang et al. \(2019\)](#) and $\sigma \sim 120\text{km/s}$ in [Wevers et al. \(2019\)](#), the BH mass from the $M_{BH} - \sigma$ relation discussed in [Zhang et al. \(2019\)](#) could be around $2.1 \times 10^6 M_\odot$ and $1.4 \times 10^7 M_\odot$, respectively. After considering the strong contributions of TDE debris to broad lines, rather than the virial BH mass, the mean BH mass about $8 \times 10^6 M_\odot$ (smaller than the virial BH mass) has been adopted through the $M_{BH} - \sigma$ relation. Then, based on the determined model parameters

in the relativistic elliptical accretion disk model, there are at least two major points we can confirm.

First, if the disk-like BLRs in SDSS J0159 was based on accreting materials from a central TDE, we would expect that the inner boundary of the disk-like BLRs could be near to (at least not very different from) the corresponding tidal disruption radius R_{TDE} . For TDEs around Schwarzschild BHs, tidal disruption radius R_{TDE} is about $R_{\text{TDE}} \sim 10R_G \times (\frac{M_{\star}}{M_{\odot}})^{-1/3} (\frac{M_{\text{BH}}}{10^7 M_{\odot}})^{-2/3} \frac{R_{\star}}{R_{\odot}}$. For SDSS J0159, Merloni et al. (2015) have shown that the central tidally disrupted star was a main-sequence star with stellar mass about (or larger) $1.2M_{\odot}$ with the virial BH mass $10^8 M_{\odot}$ accepted. However, through the $M_{\text{BH}} - \sigma$ relation, the expected BH mass is smaller than the virial BH mass, therefore, the determined stellar mass should be smaller than the value of $1.2M_{\odot}$. Then, with $M_{\text{BH}} \sim 8 \times 10^6 M_{\odot}$ and $\frac{M_{\star}}{M_{\odot}} < 1.2$, we would have $R_{\text{TDE}} < 13R_G$ similar as the model determined r_0 , strongly indicating that the model determined small inner boundary r_0 is reasonable enough, and also supporting that materials in the disk-like BLRs could be tightly related to accreting debris in a central TDE. Moreover, through the criterion that $R_{\text{TDE}} > 2R_G$, we also have the lower limit for the stellar mass is about $0.05M_{\odot}$. The following detailed descriptions to the long-term light curve by TDE models could be applied to check whether our expected stellar mass is valid.

Second, we can confirm the determined disk-like BLRs in SDSS J0159 are not similar as common BLRs in normal broad line AGN. Based on reported BLRs sizes of the reverberation mapped AGN, BLRs sizes of normal broad line AGN can be well estimated through the well-known R-L empirical relation (Bentz et al. 2013) by continuum and/or broad line luminosity. If the R-L relation was applied, the BLRs size was about 30 light-days in SDSS J0159 reported in LaMassa et al. (2015). However, based on the model determined boundaries of disk-like BLRs in SDSS J0159, the BLRs size of SDSS J0159 was about $75R_G$ (the flux-weighted radius) leading to 0.04 light-days with the BH mass about $8 \times 10^6 M_{\odot}$ accepted. Therefore, the BLRs for the observed broad $H\alpha$ of SDSS J0159 through the relativistic elliptical accretion disk model are different from the commonly expected BLRs in normal broad line AGN. The results strongly support the assumption that the broad $H\alpha$ emission materials in SDSS J0159 are from TDE debris nearer to central BH.

3 CONCLUSIONS

Finally, we give our main conclusions as follows. We can find that the relativistic elliptical disk model determined disk-like BLRs not only can be applied to well explain the asymmetric broad $H\alpha$ variabilities in SDSS J0159 indicating the disk-like BLRs are preferred, but also the determined disk-like BLRs have locations similar to the regions of accreting debris in a TDE indicating tight connections between the disk-like BLRs and TDE debris. Therefore, the well explained broad $H\alpha$ variability properties through the expected accretion disk origination actually provide further evidence to support a central TDE in the known changing-look AGN SDSS J0159.

ACKNOWLEDGEMENTS

Zhang gratefully acknowledge the anonymous referee for giving us constructive comments and suggestions to greatly improve our paper. Zhang gratefully acknowledges the kind support of Starting Research Fund of Nanjing Normal University and from the financial support of NSFC-11973029. This Letter has made use of the data from the SDSS

projects. The SDSS-III web site is <http://www.sdss3.org/>. SDSS-III is managed by the Astrophysical Research Consortium for the Participating Institutions of the SDSS-III Collaboration.

DATA AVAILABILITY

The data underlying this article will be shared on reasonable request to the corresponding author (xgzhang@njnu.edu.cn).

REFERENCES

- Bentz, M. C.; Denney, K. D.; Grier, C. J., et al., 2013, ApJ, 767, 149
 Bruzual, G.; Charlot, S. 2003, MNRAS, 344, 1000
 Chen, K. Y.; Halpern, J. P.; Filippenko, A. V., 1989, ApJ, 339, 742
 Eracleous, M.; Livio, M.; Halpern, J. P.; Storchi-Bergmann, T., 1995, ApJ, 438, 610
 Flohic, H. M. L. G.; Eracleous, M., 2008, ApJ, 686, 138
 Gezari, S.; Chornock, R.; Rest, A., et al., 2012, Nature, 485, 217
 Guillochon, J.; Ramirez-Ruiz, E., 2013, ApJ, 767, 25
 Guillochon, J.; Manukian, H.; Ramirez-Ruiz, E., 2014, ApJ, 783, 23
 Hartnoll, S. A.; Blackman, E. G., 2000, MNRAS, 317, 880
 Holoien, T. W. S.; Kochanek, C. S.; Prieto, J. L., et al., 2016, MNRAS, 455, 2918
 Holoien, T. W. S.; Huber, M. E.; Shappee, B. J., et al., 2019, ApJ, 880, 120
 Hung, T.; Foley, R. J.; Ramirez-Ruiz, E., et al., 2020, Accepted for publication in ApJ, arXiv:2003.09427
 Kauffmann, G.; Heckman, T.; Timothy, M; et al. 2003, MNRAS, 346, 1055
 Kormendy, J.; Ho, L. C., 2013, ARA&A, 51, 511
 LaMassa, S. M.; Cales C.; Moran, E. C.; et al., 2015, ApJ, 800, 144
 Liu, F. K.; Zhou, Z. Q.; Cao, R.; Ho, L. C.; Komossa, S., 2017, MNRAS Letter, 472, 99
 Loeb, A.; Ulmer, A., 1997, ApJ, 489, 573
 Merloni, A.; Dwelly, T.; Salvato, A. G.; et al., 2015, MNRAS, 452, 69
 Peterson, B. M., et al., 2004, ApJ, 613, 682
 Rees, M. J., 1988, Nature, 333, 523
 Short, P.; Nicholl, M.; Lawrence, A.; Gomez, S.; et al., 2020, MNRAS, 498, 4119
 Stone N. C.; Kesden M.; Chang R. M.; van Velzen S.; General Relativity and Gravitation, 2018, arXiv:1801.10180
 Storchi-Bergmann, T.; Nemmen da Silva, R.; Eracleous, M.; et al., 2003, ApJ, 489, 8
 Strateva, I. V., Michael A. S; Hao, L.; 2003, AJ, 126, 1720
 Thorp, S.; Chadwick, E.; Sesana, A., 2019, MNRAS, 488, 4042
 Wang, T.; Yan, L.; Dou, L., et al., 2018, MNRAS, 477, 2943
 Wang, T. G.; Dong, X. B.; Zhang, X. G., et al. 2005, ApJ Letter, 625, 35
 Wevers, T.; Nicholas C. Stone, N. C.; van Velzen, S.; et al., 2019, MNRAS, 487, 4816
 Zhang, X. G., 2013, MNRAS, 429, 2274
 Zhang, X. G., 2015, MNRAS Letter, 447, 35
 Zhang, X. G.; & Feng, L. L., 2017, MNRAS, 464, 2203
 Zhang, X. G.; & Feng, L. L., 2017b, MNRAS, 468, 620
 Zhang, X. G.; Bao, M.; Yuan, Q. R., 2019, MNRAS Letter, 490, 81